Multicritical behaviors and an induced twist grain boundary phase in a binary liquid crystalline mixture

M. Ismaïli,* A. Anakkar, G. Joly, and N. Isaert
Laboratoire de Dynamique et Structure des Matériaux Moléculaires, UPRESA CNRS No. 8024, U.F.R. de Physique, Bâtiment P5, Université des Sciences et Technologies de Lille, F59655 Villeneuve d'Ascq Cédex, France

H. T. Nguyen
Centre de Recherche Paul Pascal, Université de Bordeaux 1, F33600 Pessac, France
(Received 8 July 1999)

We report here the composition-temperature phase diagram of a mixture between $n=9$ and $n=16$ terms of a chiral tolans series shortly noted $nF_2BTFO_1M_7$. This diagram constitutes an experimental illustration of one of the three theoretical phase diagrams predicted by the Renn and Lubensky's model. The pure compounds $n=9$ and $n=16$ exhibit, respectively, the phase sequences Cry–Sm-C^*–Sm-A–TGB$_A$–N*–BP–I and Cry–Sm-C^*–N*–BP–I, where TGB refers to a twist grain boundary phase. Phases identification and transition temperatures, at atmospheric pressure, have been determined by both optical microscopy and photothermal methods. The experimental phase diagram shows the disappearance of Sm-A and TGB$_A$ mesophases and the appearance of a TGB$_C$ phase when the $n=16$ composition increases. Four of the five multicritical points theoretically anticipated by Renn and Lubensky are pointed out.

PACS number(s): 61.30.−v, 64.70.Md, 07.60.−j, 07.60.Dq

I. INTRODUCTION

In 1988, Renn and Lubensky proposed a theoretical structure of the twist grain boundary (TGB) phases [1]. They have predicted three different TGB smectics [2–4]: TGB$_A$, TGB$_C$, and TGB$_C^*$. Since the discovery of the TGB$_A$ phase by Goodby *et al.* [5] in 1989 and the TGB$_C$ phase by Nguyen *et al.* [6] in 1992, there has been an increasing interest in the physics and chemistry of the TGB phases. Several attempts have been made to predict the phase behavior on the basis of the studies of the relationship between physical properties and molecular structure in liquid crystal (LC) materials [6–8]. The result was a success since these phases (TGB$_A$ and TGB$_C$) have been found in various chiral systems [9–13] and in binary mixtures for some liquid crystalline systems based on the same nonchiral smectogenic matrix and different chiral dopants [14,15]. In binary mixtures, the behavior of pure components represents only the behavior of the system at the two extremes of the composition interval. With different compositions, a large number of other phase transitions may occur owing to the interaction of unlike or like molecules. In many cases, mixtures have properties or exhibit phenomena which are rarely present in pure component systems. For instance, the observation of a novel twist inversion in a chiral nematic phase [16] and the reentrant TGB$_A$ phase [17] have been obtained in a binary liquid crystalline mixture. Moreover, in temperature-composition phase diagrams, some phases can appear or disappear; such behavior leads to triple and/or multicritical points [18–26]. For twist grain boundary phases, in 1992, Renn [4] calculated three phase diagrams exhibiting the TGB phases in which several multicritical points were displayed. The phase diagram with only TGB$_A$ and TGB$_C$ phases is presented in Fig. 1. The multicritical points Sm-A–TGB$_A$–N* [14,16,17], Sm-C^*–Sm-A–TGB$_A$ [4,14], Sm-C^*–TGB$_C$–TGB$_A$ [6,24], TGB$_C$–TGB$_A$–N* [6], and Sm-C^*–TGB$_C$–N* [25], noted, respectively, B1, B2, B3, L, and CEP have been observed in temperature-composition phase diagrams at atmospheric pressure. In pure compounds, apart from our publications [26–28], nothing has been reported about these multicritical points at elevated pressure. No experimental temperature-composition or pressure-temperature phase diagram gathers more than three of these multicritical points.

We describe an experimentally obtained temperature-composition phase diagram analogous to a theoretical one predicted by the Renn and Lubensky model.

II. CHOICE OF COMPOUNDS

In the present work, we use several terms of the homologous series with chiral molecules: 3-fluoro-4-[(R) or (S) -methylheptyloxy] -4′-(4″- alkoxy- 2″,3″-difluorobenzoyl-

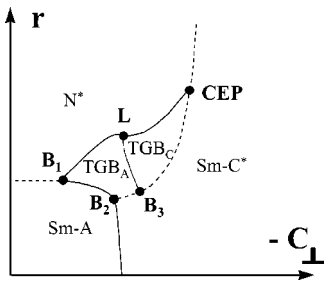

FIG. 1. Theoretical phase diagram predicted by Renn and Lubensky. Dashed lines and full lines correspond, respectively, to first order phase transitions and second order phase transitions. (Reproduced from Ref. [4].)

*Author to whom correspondence should be addressed. Electronic address: ismaili@Lip5rx.univ-lille1.fr

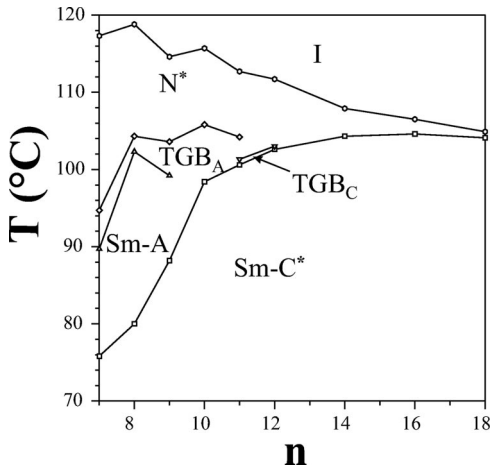

FIG. 2. Plots of the transition temperatures of the $n\mathrm{F_2BTFO_1}M_7$ compounds against n, the number of carbon atoms of the aliphatic chain.

oxy) tolans ($n\mathrm{F_2BTFO_1}M_7$ for short) whose chemical formula is [6]

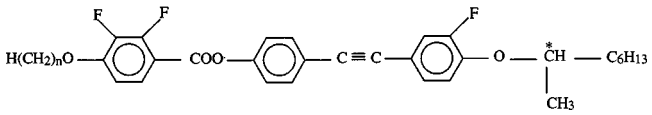

The $n=9$ term has the following phase sequences: Sm-C^*–Sm-A–TGB$_A$–N*–BP–I and the $n=16$, Sm-C^*–N*–BP–I. Phases identification and transition temperatures, at atmospheric pressure, have been determined by both thermal microscopy and differential scanning calorimetry (DSC) [6]. This series has also been studied using high resolution calorimetry [29] where more important quantity of samples and much smaller scan rates were used. The obtained results show the existence of two distinct TGB mesophases (TGB$_C^\alpha$ and TGB$_C^\beta$) and the appearance of short range TGB order in the cholesteric mesophase (chiral line liquid noted N_L^*). In the (T-n) phase diagram shown in Fig. 2, n represents the number of carbon atoms in the aliphatic chain. The transition lines which correspond to crystalline phase (Cry), blue phase (BP), and the one between the two TGB$_C$ mesophases and the chiral line liquid have not been considered. One can note that the systematic variation of aliphatic chain length considerably influences the thermal stability of the whole phases. The stability domain of TGB$_C$ phase is very narrow. The phase sequences under atmospheric pressure of homologous series can be presented in the Renn and Lubensky diagram by straight lines as shown in Fig. 3 for $n=9$ and $n=16$ compounds. Each straight line appears as defined in our previous work [26] as axis of temperature. Its positive direction is defined by the transition from an ordered phase to a disordered one. The straight line perpendicular to the temperature axis defines the n or X (concentration or composition) axis. We intend to show that the part of diagram between the straight lines of $n=9$ and $n=16$ is the (T-X) phase diagram of binary mixture for these compounds.

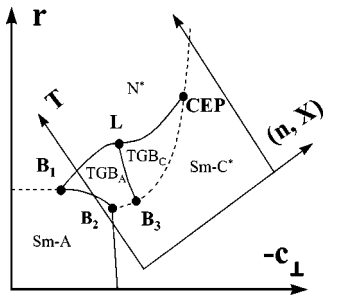

FIG. 3. Phase sequences positions for $9\mathrm{F_2BTFO_1}M_7$ and $16\mathrm{F_2BTFO_1}M_7$ characterized by the straight lines, and T and n (or composition X) axes in the phase diagram of Renn and Lubensky. The isotropic phase is not represented.

III. PHOTOTHERMAL METHOD AND SETUP DESCRIPTION

A schematic drawing of the experimental setup is shown in Fig. 4 and briefly described below: a 5 mW HeNe laser beam crosses LC cell and is detected by a photodiode. Rotating polarizer and analyzer can be added to the setup when necessary. The cell is built with two microscope slides coated to achieve a homogeneous alignment of LC. The two plates are stuck with glue to achieve a constant thickness cell. The thickness of the empty cell is determined by interferometry. All cells used in our experiments have thickness between 9 and 15 μm with an accuracy of 1 μm. The empty cell is then sandwiched between two aluminum plates, bored for light crossing and hermetically sealed with specially selected glass. Each aluminum plate is connected to two resistors to achieve homogeneous temperature in the cell. These resistors are related to a temperature controller which is connected to a thermocouple. So the sample can be heated at constant heating rates and the temperature is measured with a thermocouple near the impact point of the laser beam in the cell with an accuracy of 0.1°C. The LC cell is filled in the isotropic phase and cooled slowly to the Sm-C^* mesophase in order to achieve good orientation of the sample. Then the transmitted light intensity (TLI) through the sample cell is detected against the temperature. TLI measurements versus temperature are recorded when heating and cooling at different scan rates. For all results given in the present paper the lightening conditions are as follows.

(a) The polarizer direction is fixed in the horizontal direction and the analyzer is set to have a maximum of the TLI at the beginning of each experiment. The light beam is perpendicular to the LC cell. The experimental TLI are given in

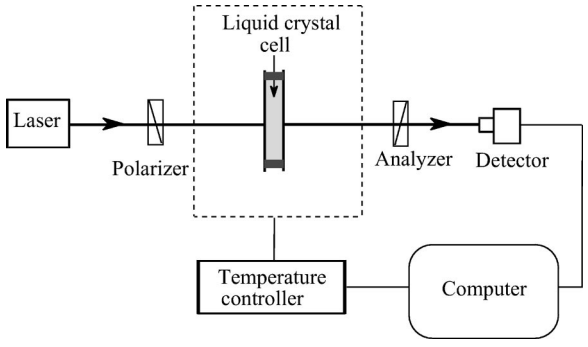

FIG. 4. Experimental setup for photothermal measurements.

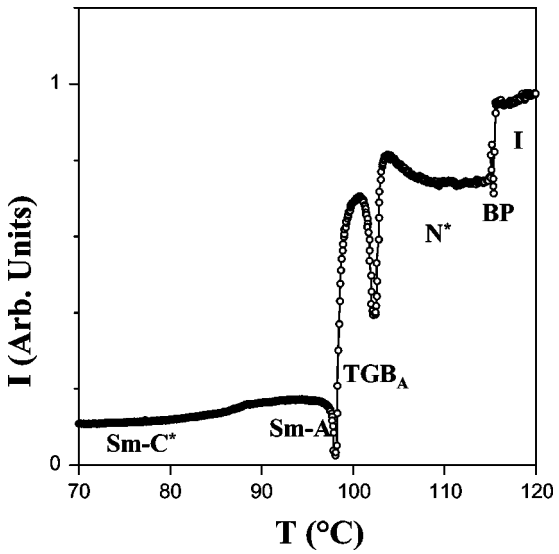

FIG. 5. Transmitted light intensity for pure compound $n=9$ $(X_{16}=0\%)$.

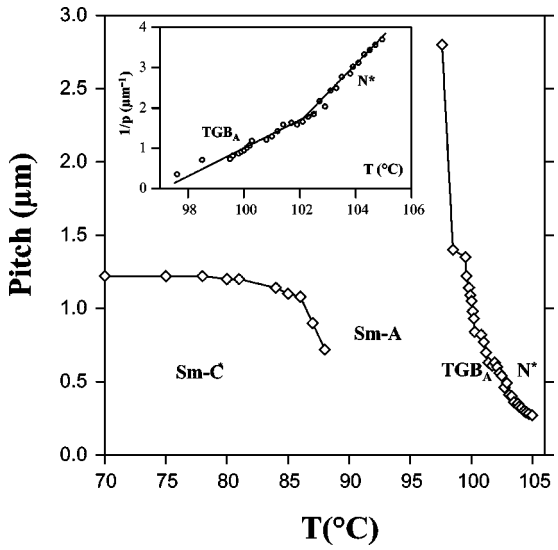

FIG. 6. Helical pitch variations according to temperature for the pure compound $n=9$. The transition temperature between TGB_A and N^* corresponds to a change of the inverse of the pitch slope.

arbitrary units and the temperature in centigrade degrees.

(b) Among the whole experiments, only those corresponding to a heating rate of 1 °C/min are presented. This choice allows comparisons between TLI measurements through differents samples.

The heating rates used in our experiments are much fast than the high resolution calorimetry rates [29]. So the chiral line liquid N_L^* has not been observed [29].

IV. RESULTS AND DISCUSSION

Our results are sorted out in accordance with the observed phase sequences. The most representative TLI are given in growing order of the mass percentage (X_{16}) of the pure compound $(n=16)$ in the mixture.

A. Sm-C^*–Sm-A–TGB_A–N*–I ($X_{16}=0\%$ and $X_{16}=10.3\%$)

The pure compound $n=9$ $(X_{16}=0\%)$ exhibits the well identified [31] Cry–Sm-C^*–Sm-A–TGB_A–N*–BP–I phase sequence. A planar alignment is achieved with usual rubbing technique. For TLI versus temperature variations, the rubbing direction of the LC cell is set parallel to the polarizer direction. Figure 5 shows the TLI data from Sm-C^* phase to isotropic one. At first sight, one can note there is a complex behavior observed within the temperature range where transitions occur. Comparison with the known phase sequence leads to an easy identification of the whole mesophases on the recorded curve. When considering that far from the transition temperatures the TLI is constant for each mesophase, the transitions are then characterized by jumps in the TLI curve except for Sm-C^*–Sm-A transition. That transition is characterized by a slight increase of the TLI in the Sm-C^* near the transition temperature and the TLI becomes approximately constant in the Sm-A mesophase. Notice that, for optical microscopy studies, it is useful to realize a pseudohomeotropic flat drop rather than a cell with planar alignment. This remark points out the sensitivity of the TLI method. In the vicinity of the Sm-A–TGB_A firstly and TGB_A–N* afterwards the situation seems to be more complicated at first sight. For the Sm-A mesophase, the TLI decrease is related to the birefringence fall versus temperature in the vicinity of the transition. At the Sm-A–TGB_A transition, the helical pitch and the block thickness are very large. When the TGB_A mesophase appears, the size of the slab width and the helical pitch tend towards finite values. The resulting abrupt increase of the TLI in the TGB_A phase is the signature of the drastic variation of the helical pitch. Near its maximum, at 99 °C, the TLI falls quickly again. This behavior is ascribed to the well-known selective reflection of the laser beam ($\lambda=632.8$ nm). Indeed, from helical pitch measurements (Fig. 6) on the pure compound, the selective reflection occurs for $p\approx 0.42$ μm nearby the TGB_A–N* transition. In the N* mesophase, a smooth decrease of the TLI is detected followed by a flat part. One can notice that the behavior of the TLI in the TGB_A and N* is similar to the rotatory power variations as a function of the inverse of the wavelength or helical pitch [30]. Just before the last transition N*–I, the TLI shows a small anomaly in the narrow interval of temperature that is consistent with the existence of the blue phase (BP) in this pure compound. The BP and Cry phases and related transitions will not be discussed, attention being focused on phase transitions involved in the Renn and Lubensky phase diagram.

To avoid problems of interpretation related to the selective reflection of the laser beam, all the following measurements are performed in homeotropic orientation. Optical microscopy observations reveal for the mixture $(X_{16}=10.3\%)$ the following phases sequence: Sm-C^*–Sm-A–TGB_A–N*–I. However, the TGB_A–N* transition is not clearly observed but looks continuous. The TLI variations versus temperature for this mixture are given in Fig. 7. In the Sm-C^*, because of the alignment and the structure of this mesophase, the wave at the exit side of the LC cell is elliptically polarized. Only a part of this wave is transmitted through the analyzer. Approaching the transition temperature, from Sm-C^*, the tilt angle decreases and falls to zero in Sm-A phase. The sample is no more birefringent and the TLI through the analyzer increases (Fig. 7). In this mixture, the

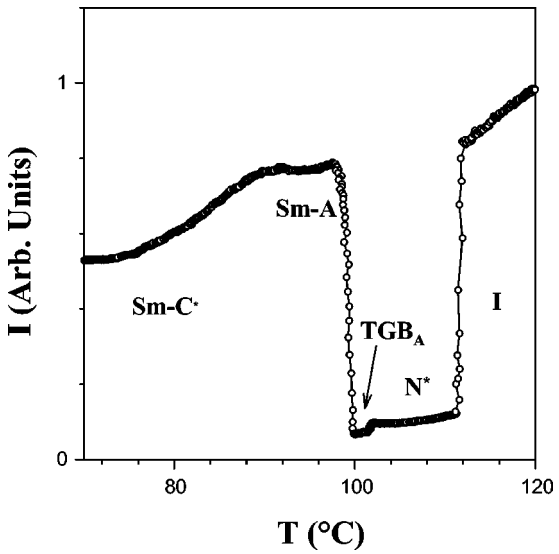

FIG. 7. Transmitted light intensity versus temperature for the mixture of $n=9$ and $n=16$ ($X_{16}=10.3\%$).

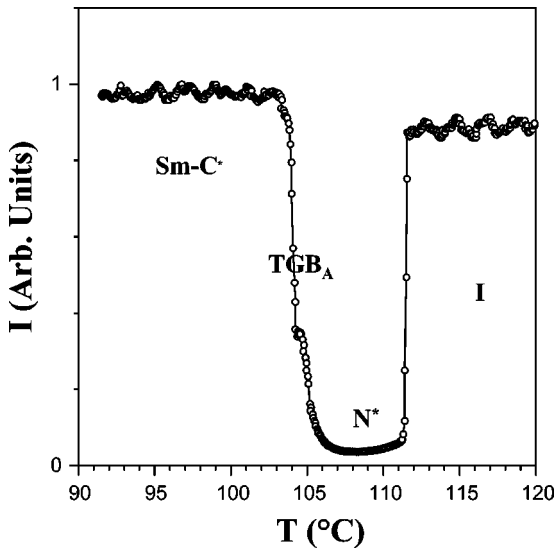

FIG. 8. Transmitted light intensity versus temperature for the mixture of $n=9$ and $n=16$ compounds ($X_{16}=28.3\%$).

domain of existence of the Sm-*A* mesophase becomes narrower than in the pure compound $n=9$. The Sm-*A*–TGB$_A$ transition is shown by an abrupt variation of the TLI. However, instead of the behavior shown in Fig. 5, the TLI decreases rapidly to reach a minimum and remains roughly constant in TGB$_A$ mesophase. These intensity variations are closely related to helical pitch variations because they change in the same way with temperature. Indeed, the sample takes on quickly a twisted structure with its screw axis in the plane of the cell. For such diffusive texture the TLI is nearly constant. There is no more decrease of TLI corresponding to the selective reflection. In the N* phase, the twist axis is also parallel to the cell faces and the TLI is also nearly constant. Since the selective reflection is eliminated by using the homeotropic orientation, the transition between TGB$_A$–N* is marked by a change in intensity level that can be ascribed to the pitch variations difference in TGB$_A$ and N* mesophases. This pitch difference appears clearly when drawing $1/p$ against temperature (as shown in Fig. 6). As in the above case, the last jump of the TLI signs the N*–I transition. Indeed both phases have no influence on the propagation of polarized light but thermal fluctuations are more important in the Sm-*A* than in the isotropic (I) phase. So the TLI is a bit higher in the I phase than in the Sm-*A* phase.

B. Sm-*C**–TGB$_A$–N*–I ($X_{16}=28.3\%$ and $X_{16}=33.2\%$)

Figure 8 shows the TLI variations for a mixture with 28.3% of the pure compound $n=16$. First of all, this curve reveals the disappearance of the Sm-*A* mesophase. The TLI through the Sm-*C** phase is a bit higher than through the isotropic one, this is consistent with the analyzer arrangement to have a maximum of the TLI at the beginning of the experiment. The first visible fall of intensity occurs at the Sm-*C**–TGB$_A$ transition. As in previous experiments, the TLI exhibits an abrupt decrease. The TGB$_A$–N* transition can now be felt in a decrease of the TLI while previously it was an increase. Optical microscopy observations show that the TGB$_A$ phase exhibits the filament texture and the N* phase the well-known fingerprint one obtained for homeotropic boundary conditions [32]. For the present mixture, there are less filaments in the TGB$_A$ phase than in the TGB$_A$ phase of the above studied mixture. So the TLI exhibits the behavior described by Fig. 8.

The domain of existence of this phase becomes narrow and will disappear for higher compositions X_{16} of the mixture. This shrinkage of the TGB$_A$ domain is confirmed by TLI variations obtained for $X_{16}=33.2\%$ (Fig. 9). Like in the former case, the TLI is weak in the N* mesophase and the *N**–I transition is expressed by a strong increase of TLI. Identical behaviors versus temperature are obtained for mixtures up to $X_{16}=44.2\%$.

C. Sm-*C**–TGB$_C$–N*–I ($X_{16}=55.4\%$ and $X_{16}=73.7\%$)

On the TLI records of these mixtures (Fig. 10), we observe a new behavior: the TLI increases when starting from

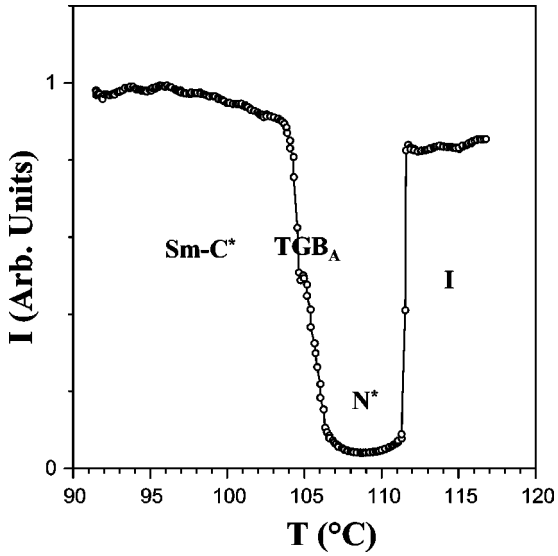

FIG. 9. Transmitted light intensity according to temperature for the mixture of $n=9$ and $n=16$ compounds ($X_{16}=33.2\%$).

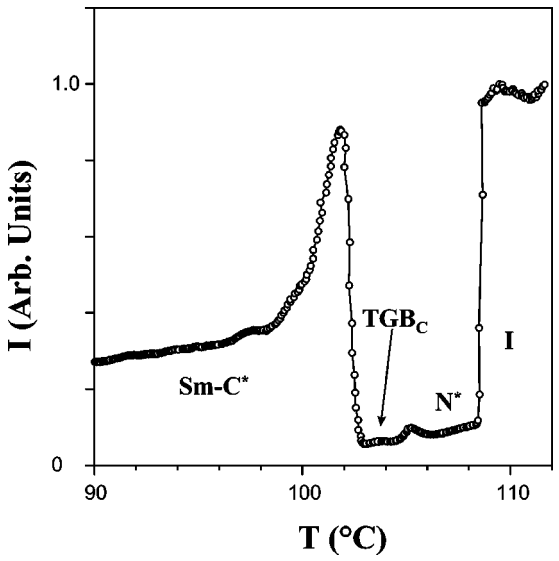

FIG. 10. Transmitted intensity versus temperature for the mixture of $n=9$ and $n=16$ compounds ($X_{16}=55.2\%$).

the Sm-C^* phase, then decreases quickly. This behavior was observed with the pure compound $n=11$ of the same chemical series, it corresponds to the Sm-C^*–TGB_C transition. The texture of the $n=11$ TGB_C mesophase has been well identified with optical microscopy observations [33]. The corresponding TLI variations with temperature at the Sm-C^*–TGB_C transition are given in Fig. 11.

In the TGB_C mesophase, as in the TGB_A one, the TLI decreases abruptly and this is consistent with the helical pitch variations versus temperature. In the Sm-C^* mesophase, towards the transition, the TLI increase can be explained by a decrease of the helical pitch. This behavior of the helical pitch, versus temperature, exists in the pure compound $n=11$ [33]. Again the twist axis of the TGB_C phase is in the cell plane and the TLI becomes nearly constant when the TGB_C texture is well organized. Finally the phase sequence of the present mixture is Sm-C^*–TGB_C–N*–I. In

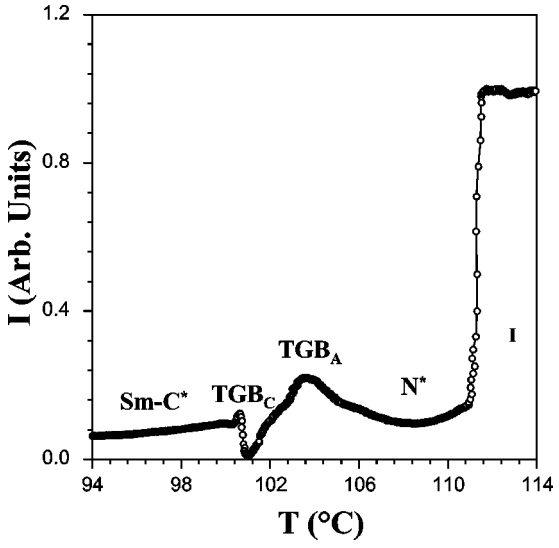

FIG. 11. Transmitted light intensity versus temperature for the pure compound $n=11$.

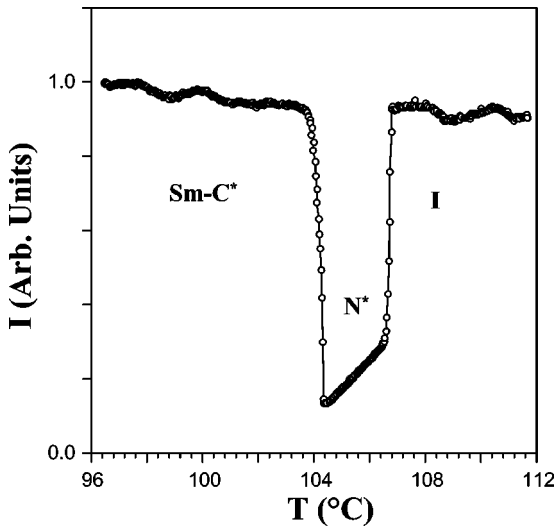

FIG. 12. Transmitted light intensity versus temperature for the mixture of $n=9$ and $n=16$ compounds ($X_{16}=83.56\%$).

the N* mesophase, the TLI is slightly higher than in the TGB_C one. The two mesophases are separated by a weak and wide peak. This peak is related to the helical pitch discontinuity at the TGB_C–N* transition temperature as observed with the pure compound $n=12$. As in previous mixtures, the N*–I transition turns up by an important increase of the TLI. When increasing the composition ($X_{16}=73.7\%$), similar variations of the TLI versus temperature are recorded with a low TLI magnitude in the Sm-C^* phase and the shrinkage of the domain of existence the TGB_C. This mesophase will vanish for higher compositions.

A. Sm-C^*–N*–I ($X_{16}=83.6\%$ and $X_{16}=100\%$)

At high compositions in $n=16$ compound (mixtures with X_{16} higher than 83.6%), only Sm-C^* and N* mesophases exist (Fig. 12). The TLI values in the Sm-C^* and isotropic phases are of the same magnitude and stronger than in the N* mesophase. In the N*, the TLI is approximately constant for the pure compound and evolves with temperature for the mixture $X_{16}=83.6\%$. This means that the helical pitch variations versus temperature are weaker in pure compound than in mixtures. As a remark on the accuracy of the method, notice that the transition temperatures of the pure compound, are consistent with those determined by DSC elsewhere [31].

V. PHASE DIAGRAM AND DISCUSSION

The above results obtained with various mixtures enable to draw the composition-temperature phase diagram (Fig. 13) between two compounds characterized by the following phase sequences Sm-C^*–Sm-A–TGB_A–N* and Sm-C^*–N*. It is interesting now to discuss this diagram in more details.

The first three mixtures ($X_{16}=0$, 10.3, and 19.3%) exhibit, as illustrated in the phase diagram, the Sm-C^*–Sm-A–TGB_A–N* phase sequence. As one can see, both domains of TGB_A and Sm-A mesophases decrease

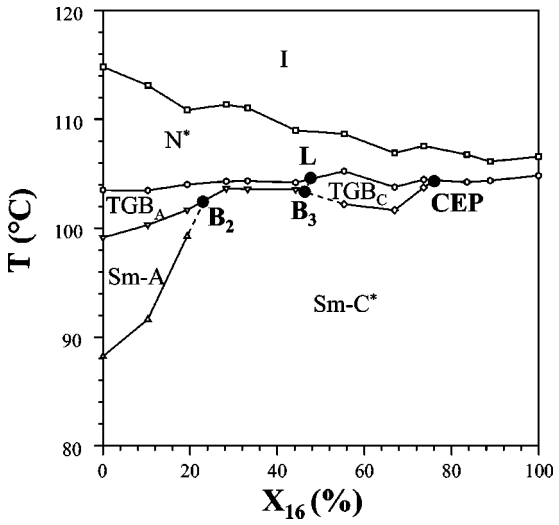

FIG. 13. Temperature-composition (T,X) phase diagram of the binary systems $9F_2BTFO_1M_7$ and $16F_2BTFO_1M_7$. Here X_{16} indicates the mass percentage of the pure compound $16F_2BTFO_1M_7$ in the mixture. The different phases are isotropic (I), cholesteric (N*), twist grain boundary phases (TGB_A and TGB_C), smectic A (Sm-*A*) and smectic *C** (Sm-*C**).

when increasing the composition X_{16}. Note also that the Sm-*A* domain decreases faster than the TGB_A one.

The Sm-*C**–TGB_A–N* phase sequence appears for $X_{16}=28.3$, 33.2, and 44.2 % mixtures. The Sm-*A* mesophase disappears between $X_{16}=19.3$ and 28.3 % mixtures. This disappearance corresponds to the existence of a Sm-*C**–Sm-*A*–TGB_A multicritical point. It represents the intersection of the Sm-*C**–Sm-*A*, Sm-*A*–TGB_A, and Sm-*C**–TGB_A phase boundaries and is denoted B2 in the Renn and Lubensky theoretical phase diagram. Even if it seems that the TGB_A domain remains constant, the TLI curves confirm that it diminishes more and more as the composition rises.

The mixtures $X_{16}=55.4$, 67, and 73.7 % exhibit Sm-*C**–TGB_C–N* phase sequences. The TGB_C mesophase has appeared in binary mixture even though neither component shows this mesophase. On the other hand, the TGB_A mesophase has completely disappeared by increasing the composition. That is to say a TGB_A–TGB_C transition line has to exist in the diagram somewhere between 44.2 and 55.4 % values of the X_{16} composition. This line must intersect the Sm-*C**–TGB_A line and the TGB_A–N* one. Consequently, this induces the existence of two multicritical points. One of them, where the three phase boundaries Sm-*C**–TGB_C, Sm-*C**–TGB_A, and TGB_C–TGB_A meet, is the Sm-*C**–TGB_C–TGB_A point denoted B3 by Renn and Lubensky. The other point TGB_C–TGB_A–N* denoted L is the only common intersection point of the TGB_C–TGB_A, TGB_C–N*, and TGB_A–N* phase boundaries. As shown in the experimental phase diagram, the B3 point must be on the left of the L point, since the TGB_C mesophase would precede the TGB_A one as the temperature rises. It follows then that between these two multicritical points, the phase sequence Sm-*C**–TGB_C–TGB_A–N* has to happen.

The last three mixtures ($X_{16}=83.6$, 88.9, and 100 %) display the Sm-*C**–N* phase sequence. The further important fact here is the absence of the TGB_C mesophase. Its disappearance by increasing the X_{16} composition requires the existence of a Sm-*C**–TGB_C–N* multicritical point between $X_{16}=73.7\%$ and $X_{16}=83.6\%$ compositions. This point denoted CEP represents the intersection of Sm-*C**–TGB_C, Sm-*C**–N* and TGB_C–N* phase boundaries.

We now turn our attention to discuss the connection between the $(T\text{-}X)$, $(T\text{-}n)$, and $(r,\text{-}C_\perp)$ phase diagrams. We can note that the $(T\text{-}X)$ and $(T\text{-}n)$ phase diagrams have the same basic topology. So they are similar, which means that the same phases are present and relationships between them are the same. We could even argue that these two diagrams are not only qualitatively but also quantitatively similar inasmuch as they differ simply by the scale factor relating the carbon number (n) to composition (X) changes. Concerning the theoretical diagram $(r,\text{-}C_\perp)$, it is qualitatively similar to the $(T\text{-}X)$ experimental one inasmuch as each diagram could be deduced from another one by appropriate rotation and translation of the phase diagram axes (Fig. 3) . Thus, we would conclude that the $(T\text{-}X)$ and $(T\text{-}n)$ phase diagrams are the analogs of the $(r,\text{-}C_\perp)$ theoretical one predicted by Renn and Lubensky's model. To sum up, by using a homologous series exhibiting the following phase sequences versus the aliphatic chain lengths: Sm-*C**–Sm-*A*–N*, Sm-*C**–Sm-*A*–TGB_A–N*, Sm-*A*–TGB_A–N*, Sm-*C**–TGB_C–TGB_A–N*, Sm-*C**–TGB_C–N* and TGB_C–N*, the mixture of two compounds which display the first and last phase sequences will lead to a $(T\text{-}X)$ phase diagram with the five multicritical points of the model.

VI. CONCLUSION

Transmitted light intensity measurements versus temperature have been performed on mixtures between $n=9$ and $n=16$ terms of the homologous series of chiral liquid crystals $nF_2BTFO_1M_7$. The TLI records enable us to characterize the phase sequences of the mixtures. For these experiments it is better to adopt the homeotropic orientation of the sample in order to overcome interpretation problems related to the selective reflection. This photothermal technique allowed us to draw quickly the temperature-composition phase diagram of the two compounds. The experimental phase diagram shows the disappearance of Sm-*A* and TGB_A mesophases and the appearance of a TGB_C one. Four multicritical points Sm-*C**–Sm-*A*–TGB_A, Sm-*C**–TGB_C–TGB_A, TGB_C–TGB_A–N*, Sm-*C**–TGB_C–N*, noted, respectively, B2, B3, L, and CEP have been put in evidence together. The obtained experimental phase diagram is the analog of a theoretical one predicted by Renn and Lubensky's model.

ACKNOWLEDGMENT

We would like to thank A. Deppière from the Laboratoire de Modalité du Fictionnel, ULCO, Dunckerque for her assistance.

[1] S. R. Renn and T. C. Lubensky, Phys. Rev. A **38**, 2132 (1988).
[2] T. C. Lubensky and S. R. Renn, Phys. Rev. A **41**, 4392 (1990).
[3] R. Renn and T. C. Lubensky, Mol. Cryst. Liq. Cryst. **209**, 349 (1991).
[4] S. R. Renn, Phys. Rev. A **45**, 953 (1992).
[5] J. W. Goodby, M. A. Waugh, S. M. Stein, E. Chin, R. Pindak, and J. S. Patel, Nature (London) **337**, 449 (1989).
[6] H. T. Nguyen, A. Bouchta, L. Navailles, P. Barois, N. Isaert, R. J. Twieg, A. Maaroufi, and C. Destrade, J. Phys. II **2**, 1889 (1992).
[7] A. Bouchta, H. T. Nguyen, M. F. Achard, F. Hardouin, C. Destrade, R. J. Twieg, A. Maaroufi, and N. Isaert, Liq. Cryst. **12**, 575 (1992).
[8] J. W. Goodby, I. Nishiyama, A. J. Slaney, C. J. Booth, and K. J. Toyne, Liq. Cryst. **14**, 37 (1993).
[9] I. Dierking, F. Gießelmann, and P. Zugenmaier, Liq. Cryst. **17**, 17 (1994).
[10] A. C. Ribeiro, A. Dreyer, L. Oswald, J. F. Nicoud, A. Soldera, D. Guillon, and Y. Galerne, J. Phys. II **4**, 407 (1994).
[11] S. L. Wu and W. J. Hsieh, Liq. Cryst. **23**, 783 (1996).
[12] H. T. Nguyen, A. Babeau, J. C. Rouillon, G. Sigaud, N. Isaert, and F. Bougrioua, Ferroelectrics **179**, 33 (1996).
[13] M. H. Li, V. Laux, H. T. Nguyen, G. Sigaud, Ph. Barois, and N. Isaert, Liq. Cryst. **23**, 389 (1997).
[14] N. L. Kramarenko, G. P. Semenkova, V. I. Kulishov, A. S. Tolochko, L. A. Kutulya, V. V. Vaschenko, and T. V. Handrimajlova, Liq. Cryst. **17**, 351 (1994).
[15] N. L. Kramarenko, V. I. Kulishov, L. A. Kutulya, V. P. Seminozhenko, and N. I. Shkolnikova, Liq. Cryst. **22**, 535 (1997).
[16] C. J. Booth, J. W. Goodby, J. P. Hardy, and K. J. Toyne, Liq. Cryst. **16**, 43 (1994).
[17] V. Vill, H. W. Tunger, and D. Peters, Liq. Cryst. **20**, 547 (1996).
[18] P. H. Keyes, H. T. Weston, and W. B. Daniels, Phys. Rev. Lett. **31**, 628 (1973).
[19] D. Dehoff, R. Biggers, D. Brisbin, R. Mahmood, C. Gooden, and D. L. Johnson, Phys. Rev. Lett. **47**, 664 (1981).
[20] C. R. Safinya, R. J. Birgeneau, and J. D. Litster, Phys. Rev. Lett. **47**, 668 (1981).
[21] R. Shashidhar, B. R. Ratna, and S. Krishna Prasad, Phys. Rev. Lett. **53**, 2141 (1984).
[22] W. Pyzuk, E. Gorecka, J. Szydlowska, A. Krowczynski, D. Pociecha, and J. Przedmojski, Phys. Rev. E **52**, 1748 (1995).
[23] S. Krishna Prasad, D. S. Shankar Rao, S. Chandrasekhar, M. E. Neubert, and J. W. Goodby, Phys. Rev. Lett. **74**, 270 (1995).
[24] M. Werth, H. T. Nguyen, C. Destrade, and N. Isaert, Liq. Cryst. **17**, 863 (1994).
[25] H. Yoshida, Phys. Lett. A **172**, 267 (1993).
[26] A. Anakkar, N. Isaert, M. Ismaïli, J.-M. Buisine, and H. T. Nguyen, Phys. Rev. E **60**, 620 (1999).
[27] A. Anakkar, A. Daoudi, J.-M. Buisine, N. Isaert, F. Bougrioua, and H. T. Nguyen, Liq. Cryst. **20**, 411 (1996).
[28] A. Anakkar, A. Daoudi, J.-M. Buisine, N. Isaert, T. Delattre, H. T. Nguyen, and C. Destrade, J. Therm. Anal. **41**, 1501 (1994).
[29] L. Navailles, C. W. Garland, and H. T. Nguyen, J. Phys. II **6**, 1243 (1996).
[30] H. De Vries, Acta Phys. Pol. **4**, 219 (1951).
[31] A. Bouchta, H. T. Nguyen, L. Navailles, P. Barois, C. Destrade, F. Bougrioua, and N. Isaert, J. Mater. Chem. **5**, 2079 (1994).
[32] I. Dierking and S. T. Lagerwall, Liq. Cryst. **26**, 83 (1999).
[33] N. Isaert, L. Navailles, P. Barois, and H. T. Nguyen, J. Phys. II **4**, 1501 (1994).